Nonlinear Exceptional Points with a Complete Basis in Dynamics

Kai Bai,[1] Jia-Zheng Li,[1] Tian-Rui Liu,[1] Liang Fang,[1] Duanduan Wan,[1,*] and Meng Xiao[1,2,†]
[1]Key Laboratory of Artificial Micro- and Nano-structures of Ministry of Education and School of Physics and Technology, Wuhan University, Wuhan 430072, China
[2]Wuhan Institute of Quantum Technology, Wuhan 430206, China

(Received 13 January 2023; revised 13 April 2023; accepted 8 June 2023; published 29 June 2023)

Exceptional points (EPs) are special spectral singularities at which two or more eigenvalues, and their corresponding eigenvectors, coalesce and become identical. In conventional wisdom, the coalescence of eigenvectors inevitably leads to the loss of completeness of the eigenbasis. Here, we show that this scenario breaks down in general at nonlinear EPs (NEPs). As an example, we realize a fifth-order NEP (NEP_5) within only three coupled resonators with both a theoretical model and simulations in circuits. One stable and another four auxiliary steady eigenstates of the nonlinear Hamiltonian coalesce at the NEP_5, and the response of eigenfrequency to perturbations demonstrates a fifth-order root law. Intriguingly, the biorthogonal eigenbasis of the Hamiltonian governing the system dynamics is still complete, and this fact is corroborated by a finite Petermann factor instead of a divergent one at conventional EPs. Consequently, the amplification of noise, which diverges at other EPs, converges at our NEP_5. Our finding transforms the understanding of EPs and shows potential for miniaturizing various key applications operating near EPs.

DOI: 10.1103/PhysRevLett.130.266901

Introduction.—The exotic physics at singularities is always under the scrutiny of theoretical and experimental investigations. Exceptional points (EPs) are unique singularities in non-Hermitian systems [1–3] where two or more eigenvalues and their corresponding eigenvectors coalesce [3–5]. After being experimentally demonstrated in microwave cavities [6], EPs were subsequently observed in various systems [7–18]. Many exciting physics and novel phenomena related to EPs have been elucidated [19–26]. For example, the spectra exhibit algebraic singularities at the EPs, which are responsible for amplifying a detected signal [13,16]. Meanwhile, a dynamic loop near an EP leads to chiral state transfer [19–22], and this unique feature enables various nontrivial functionalities [21–25].

These EP-related advances have enriched our understanding of complex systems with nonconservative elements (gain, loss, and nonreciprocal coupling) and brought many fascinating potential applications. However, some fundamental challenges remain, especially when considering miniaturizing the device in practical schemes. On the one hand, previous studies mainly focused on linear systems, where system parameters are independent of the fields' amplitudes. The detectable signal dissipates rapidly in a passive system. Including gain elements increases the system's complexity in structural optimization and noise control. Meanwhile, a proper description of systems with gain elements unavoidably involves nonlinear effects such as gain saturation and Kerr nonlinearity [27,28]. Then the outcome deviates from the prediction of the linear model [29–34]. Nevertheless, research combining nonlinearity, parity-time symmetry, and EPs is rare [35–39]. On the other hand, signal amplification [13,16–18] and chiral states transfer [19–22] require operations pretty close to the EPs, which demands tedious and precise parameter control, especially when higher-order EPs get involved [13,40–42]. Moreover, the unavoidable noise is dramatically increased near conventional linear EPs due to the loss of the completeness of eigenbasis [43–46]. The above conflicts seem irreconcilable and generally require brilliant schemes for EP-related operations [22,47]. It is thus natural to ask: Can the completeness of the eigenbasis be revived while the key features of EPs are still preserved?.

Here in this work, we present a nonlinear route to overcome this dilemma. In analogy with laser theory [29,48], a Hamiltonian with nonlinear saturable gain has some steady eigenmodes whose frequencies satisfy a polynomial equation with real coefficients. Thus, the solutions of this polynomial equation are either real or come in complex conjugate pairs. This nonlinear Hamiltonian can be mapped into a higher dimensional parity-time (PT) symmetric linear Hamiltonian [31,49]. Under this mapping, the phase transition point, EP, of the PT-symmetrical linear Hamiltonian corresponds to a unique singularity of the nonlinear Hamiltonian. Corresponding to the coalescence of the PT-symmetrical linear Hamiltonian eigenmodes at the EPs, some (auxiliary) steady eigenmodes of the nonlinear Hamiltonian become identical at this singularity. Therefore, we name it nonlinear exceptional point (NEP) with an additional "N" denoting nonlinearity. Across the NEPs, the number of steady eigenmodes with real frequency can

change. Meanwhile, the dynamical evolution of the nonlinear system is governed by the instantaneous Hamiltonian, whose eigenstates are generally different from the steady eigenmodes to form the NEP. (Note that as the nonlinear Hamiltonian depends on the instantaneous state of the system, different eigenmodes can correspond to different instantaneous Hamiltonians.) Remarkably, this fact allows us to design a NEP while the instantaneous Hamiltonian exhibits a complete basis in dynamics.

To illustrate the physics discussed above, we propose a general scheme to construct a NEP with a complete basis in dynamics. However, to keep our formulas and text neat and concise, we choose a fifth-order NEP (NEP_5) as an example and leave the general form to the Supplemental Material, Sec. 1 [50]. We construct this NEP_5 based on three coupled resonators combined with a nonlinear saturable gain, and verify our conclusions with both a model Hamiltonian and circuit simulations. At the NEP_5, one steady stable and four auxiliary eigenmodes become identical, and the response of eigenfrequencies demonstrates a fifth-order root law. Owing to the feedback mechanism of the saturable gain, the system can fall back to one of the stable eigenmodes in a short time and remains at that eigenmode thereafter. Consequently, the temporal dynamics of the system at the NEP_5 is governed entirely by the instantaneous Hamiltonian anchored by the stable eigenmode. Intriguingly, this instantaneous Hamiltonian is diagonalizable, i.e., the eigenbasis is complete. The Petermann factor (PF), which measures the nonorthogonality of the eigenbasis in an experimentally friendly manner, converges. Thus, the adverse effects of noise are largely suppressed from a fundamental perspective.

Hamiltonian exhibiting NEP_5.—Our system is sketched in Fig. 1(a). The nonlinear Schrödinger equation is

$$H_{|\boldsymbol{\psi}^{\boldsymbol{R}}\rangle}|\boldsymbol{\psi}^{\boldsymbol{R}}\rangle = \omega|\boldsymbol{\psi}^{\boldsymbol{R}}\rangle, \tag{1}$$

where ω is the eigenfrequency. $|\boldsymbol{\psi}^{\boldsymbol{R}}\rangle \equiv (\psi_A, \psi_B, \psi_C)^T$ is the right eigenstate with superscript T short for transpose, and ψ_A, ψ_B, and ψ_C representing the field amplitude of the red (left), blue (middle), and light red (right) resonators A, B, and C, respectively. And the tight-binding Hamiltonian $H_{|\boldsymbol{\psi}^{\boldsymbol{R}}\rangle}$ can be written as

$$H_{|\boldsymbol{\psi}^{\boldsymbol{R}}\rangle} = \begin{pmatrix} \omega_A + ig_A(|\psi_A|) & \kappa_1 & 0 \\ \kappa_1 & \omega_B - il_B & \kappa_2 \\ 0 & \kappa_2 & \omega_C + ig_C \end{pmatrix}, \tag{2}$$

where ω_A, ω_B, and ω_C represent the corresponding resonant frequencies, respectively. $g_A(|\psi_A|)$ denotes a nonlinear saturable gain which decreases with the increasing of $|\psi_A|$. In optics, a commonly used gain saturation model is $g_A(|\psi_A|) = \Gamma/(1 + |\psi_A|^2) - \gamma_0$ with Γ representing the pump strength and γ_0 representing the intrinsic loss. l_B and g_C represent the linear loss in resonator B and the linear gain in resonator C, respectively. Here the nonlinearity of the gain g_C is ignored, which is appropriate when the stable value of $|\psi_C|$ is much smaller than the saturation amplitude of the gain profile in resonator C. κ_1 and κ_2 are the corresponding coupling strength. All the parameters are normalized by κ_1, and we set ω_A to 0 since any global frequency shift is irrelevant. Focusing on the stable state reached, the eigenfrequency ω satisfies a fifth-order equation

$$\begin{aligned} p(\omega) = {} & \omega|\mathrm{Det}(H_{B-C} - \omega\mathbf{I})|^2 \\ & + \mathrm{Im}[\mathrm{Det}(H_C - \omega\mathbf{I})] * \mathrm{Im}[\mathrm{Det}(H_{B-C} - \omega\mathbf{I})] \\ & + \mathrm{Re}[\mathrm{Det}(H_C - \omega\mathbf{I})] * \mathrm{Re}[\mathrm{Det}(H_{B-C} - \omega\mathbf{I})] \\ = {} & \omega^5 + x_4\omega^4 + x_3\omega^3 + x_2\omega^2 + x_1\omega + x_0 = 0, \end{aligned} \tag{3}$$

and the corresponding saturated gain value g_s is determined by

$$\begin{aligned} & g_s\mathrm{Re}[\mathrm{Det}(H_{B-C} - \omega\mathbf{I})] - \omega\mathrm{Im}[\mathrm{Det}(H_{B-C} - \omega\mathbf{I})] \\ & - \mathrm{Im}[\mathrm{Det}(H_C - \omega\mathbf{I})] = 0; \end{aligned} \tag{4}$$

here $\mathbf{I}$ is the identity matrix.

$$H_{B-C} = \begin{pmatrix} \omega_B - il_B & \kappa_2 \\ \kappa_2 & \omega_C + ig_C \end{pmatrix} \tag{5}$$

represents the tight-binding Hamiltonian of a subsystem consisting of the resonators B and C; $H_C = (\omega_C + ig_C)$ denotes the on site term of the resonator C. $\{x_0, \ldots, x_4\}$ are

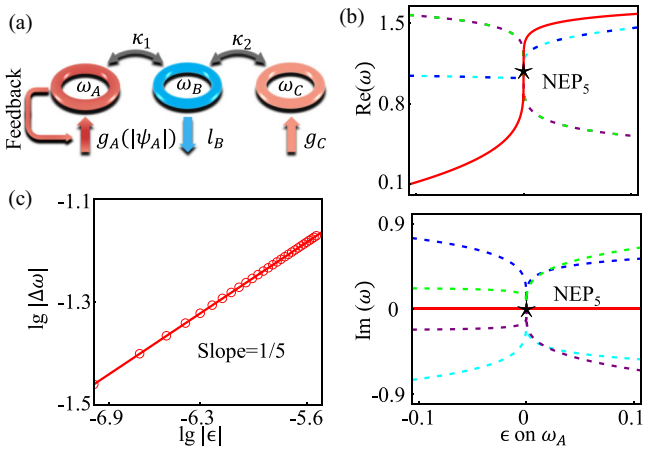

FIG. 1. (a) Schematic of our model. The nonlinear gain $g_A(|\psi_A|)$ depends on $|\psi_A|$. (b) Eigenvalues versus the external perturbation ϵ, where the solid red line and four dashed (cyan, blue, purple, and green) lines represent the stable and four auxiliary modes, respectively. (c) The critical behavior of the stable mode near the NEP_5. Here the circles are from the red line in (b), and the solid line represents a straight line with a slope 1/5. The parameters used are $\omega_B = 1.18$, $\omega_C = 1.53$, $l_B = 2.87$, $g_C = 1.25$, $\kappa_2 = 2$.

real functions in the $(\omega_B, \omega_C, l_B, g_C, \kappa_2)$ space. Their explicit forms are provided in the Supplemental Material, Sec. 2 [50]. Here, the gain saturation form is irrelevant to the order of $p(\omega)$. We analyze all the possible fifth-order multiple roots of $p(\omega)$ and choose the combination of parameters where the roots are stable. Let ϵ represent the external perturbation of the system parameters to those at the fifth-order multiple roots ω_0. Near ω_0, the response of eigenfrequency $\Delta\omega \equiv \omega - \omega_0$ for ϵ is proportional to $\sqrt[5]{\epsilon}$ if $\partial_\epsilon p(\omega) \neq 0$. (Detailed proof is provided in the Supplemental Material, Sec. 2 [50].) The improved responsivity, $\partial_\epsilon \Delta\omega$, is highly desirable in amplifying a detected perturbation ϵ [13,16]. In the main text, ϵ is imposed on ω_A for demonstration purposes, i.e., $\omega_A + \epsilon$. We note that single-mode systems with Kerr nonlinearity can improve the sensing in noisy environments [51]. In addition to extraordinary sensitivity enhancement, our approach based on NEPs with multimode systems is robust and flexible to achieve various applications explored in conventional linear EPs [19–25].

To understand the underlying physics, we extend the solutions search of the polynomial [Eq. (3)] to the complex plane. In Fig. 1(b), the solid red lines correspond to stable modes and the other lines to the other four auxiliary modes. Figure 1(c) shows the critical component of the $\Delta\omega$ versus ϵ for the stable mode (open circles), which fits well with $\sqrt[5]{\epsilon}$ (the red line). Substituting the ω obtained above and the corresponding gain g_s into Eq. (1), the eigenstates can be obtained (see Fig. S3 of the Supplemental Material [50]). It is clear that one stable eigenmode and four auxiliary eigenmodes become identical at this special singularity NEP_5. The five eigenvalues in Fig. 1(b) are either real or come in complex conjugate pairs. These eigenvalues and the corresponding eigenstates can be mapped into a PT-symmetric linear Hamiltonian [31,49]. Compared with the conventional linear systems, the parameters required to reach an EP_5 are reduced from 12 in conventional systems to five in our system. Note that, for the four auxiliary eigenmodes in Fig 1, the corresponding g_s are complex. In contrast, $g_A(|\psi_A|)$ for most of the common gain models [29–31] is purely real. Thus, the four auxiliary eigenvalues (eigenstates) are unphysical, but their presence is crucial to understanding the NEP_5.

In conventional wisdom, the orthogonality of eigenstates gradually diminishes as one approaches the EPs, and the eigenbasis is incomplete. The loss of orthogonality can be captured with [46]

$$\chi = 1 - \overline{\{|\langle \boldsymbol{\psi}_\alpha^{\boldsymbol{R}} | \boldsymbol{\psi}_\beta^{\boldsymbol{R}} \rangle|\}}, \tag{6}$$

where each eigenstate is prenormalized as $\langle \boldsymbol{\psi}_\alpha^{\boldsymbol{R}} | \boldsymbol{\psi}_\alpha^{\boldsymbol{R}} \rangle = 1$, $\overline{\{\bullet\}}$ represents the algebraic average of the set $\{\bullet\}$, and the subscript $\alpha, \beta = \{1, \ldots, n\}$ denote different eigenstates

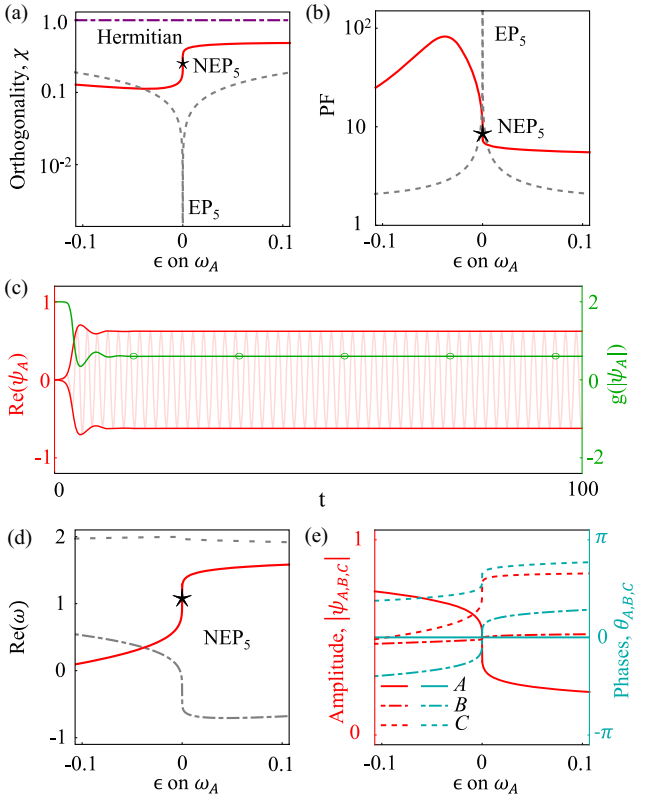

FIG. 2. (a) Orthogonality function χ for a Hermitian system (dot-dashed purple line), a PT-symmetric Hamiltonian in Eq. (S11) (dashed gray line), and our system (solid red line). Here, χ does not reach 1 as the parameters are not far enough from all the possible EPs in the parameter space. (b) PF of the stable state (solid red line) at the NEP_5 is finite, contrasting sharply with a divergent one for the linear system (dashed gray line). (c) Evolution of $\mathrm{Re}(\psi_A)$ (red line) and $g_A(|\psi_A|)$ (dark green line) starting from a small initial state $(10^{-3}, 10^{-3}, 10^{-3})^T$. In a short time, the nonlinear system will reach a stable state. The $g_A(|\psi_A|)$ (dark green) matches g_s obtained from Eq. (4) (dark green circles). (d) The real part of the eigenvalues of H_s. (e) The amplitude and phase distribution of the stable state. The parameters for the linear system are provided in the Supplemental Material, Sec. 2 [50]. Parameters of the nonlinear system in (a), (b),(d),(e) are the same as those in Fig. 1. The parameters used in (c) are $\omega_A = 2.9$, $\omega_B = 4.18$, $\omega_C = 4.53$, $l_B = 2.87$, $g_C = 1.25$, $\kappa_2 = 2$, and $g_A = 5/(1 + |\psi_A|^2) - 3$.

with $\alpha > \beta$ and n denoting the dimension. All eigenstates are orthogonal to each other for Hermitian Hamiltonians, i.e.,$\langle \boldsymbol{\psi}_\alpha^{\boldsymbol{R}} | \boldsymbol{\psi}_\beta^{\boldsymbol{R}} \rangle = \delta_{\alpha,\beta}$, and thus $\chi \equiv 1$ as depicted by the purple dot-dashed line in Fig. 2(a). In contrast, all eigenstates become identical, i.e., $\langle \boldsymbol{\psi}_\alpha^{\boldsymbol{R}} | \boldsymbol{\psi}_\beta^{\boldsymbol{R}} \rangle = \langle \boldsymbol{\psi}_\alpha^{\boldsymbol{R}} | \boldsymbol{\psi}_\alpha^{\boldsymbol{R}} \rangle = 1$ at conventional EPs in linear systems. As a result, $\chi = 0$ at a linear EP_5 as shown by the gray dashed line in Fig. 2(a). The loss of orthogonality in the vicinity of EPs dramatically increases the adverse effects of noise and has triggered an ongoing debate in the EP-related sensing protocols [13,16,43–46,56]. The enhancement of noise for an

eigenmode $|\boldsymbol{\psi}^{\boldsymbol{R}}\rangle$ is conventionally characterized by the PF [43–45], a measure of nonorthogonality:

$$\mathrm{PF} \equiv 1/|\langle \boldsymbol{\psi}^{\boldsymbol{L}}|\boldsymbol{\psi}^{\boldsymbol{R}}\rangle|^2. \tag{7}$$

The corresponding left eigenstate $\langle \boldsymbol{\psi}^{\boldsymbol{L}}|$ is also prenormalized. Since the left and right eigenstates are self-orthogonal at conventional linear EPs, the PF diverges when approaching a conventional linear EP as shown by the dashed gray line in Fig. 2(b).

The above scenario for conventional linear EPs can break down at NEPs. The (auxiliary) steady eigenmodes of Eq. (1) can correspond to different Hamiltonians as $H_{|\boldsymbol{\psi}^{\boldsymbol{R}}\rangle}$ depends on $|\boldsymbol{\psi}^{\boldsymbol{R}}\rangle$. Hence the (auxiliary) steady eigenmodes becoming identical at NEPs does not necessarily lead to the coalescence of the eigenmodes of the instantaneous Hamiltonian, which governs the system dynamics. More specifically, each solution of Eq. (3) can correspond to a different gain value as given by Eq. (4). However, the nonlinear system will reach one of the steady stable modes (if it exists) in a short time due to the feedback mechanism [29–31,57], and the nonlinear gain coefficient $g_A(t)$ is anchored by the stable mode at a stable value g_s. Thereafter, the temporal dynamics is governed by a 3×3 instantaneous Hamiltonian H_s with the saturable gain replaced by g_s and subjected to noise-imposed fluctuations. Generally, H_s does not exhibit an EP point though (auxiliary) steady eigenmodes coalesce at the NEPs. Hence, the PF factor, which characterizes the noise dynamics within the space governed by H_s, does not diverge.

To unveil this fact more explicitly, we still use the three-resonator system in Fig. 1(a). The red and dark green lines in Fig. 2(c) show the $\mathrm{Re}(\psi_A)$ and g_A by solving the time-dependent nonlinear Schrödinger equation $i\partial_t|\boldsymbol{\psi}^{\boldsymbol{R}}\rangle = H_{|\boldsymbol{\psi}^{\boldsymbol{R}}\rangle}|\boldsymbol{\psi}^{\boldsymbol{R}}\rangle$ starting from a small initial state. After a short time, the gain stays at a stable value g_s (green circles) as defined in Eq. (4). We emphasize that the stable state reached is also an eigenstate of H_s. Besides the stable state, there are another two eigenstates of H_s. Figure 2(d) shows the real part of the eigenvalues of H_s, with the solid red line representing the same stable mode as shown in Fig. 1(b) and the dot-dashed and dashed gray lines denoting the other two eigenvalues of H_s. Figure 2(e) shows the normalized field amplitudes $\{|\psi_A|, |\psi_B|, |\psi_C|\}$ and relative phases $\{\theta_A, \theta_B, \theta_C\}$ of the stable mode. The fields of the other two eigenstates are provided in Fig. S5. It is clear that the three eigenstates of H_s do not coalesce at the NEP_5. Substituting the three eigenstates into Eq. (6), we see that χ is nonzero at the NEP_5 [the red line in Fig. 2(a)]. In other words, the eigenbasis of H_s is still complete at the NEP_5, which is in stark contrast to linear Hamiltonians at conventional EPs. We also calculate the PF factor for the stable state as shown with the red line in Fig. 2(b). These results verify our core conclusion that the completeness of the eigenbasis can be recovered and the PF is finite with a nonlinear saturable gain. We note that there have been a few delicate schemes to compensate for the adverse consequence due to the loss of complete basis: shifting from EPs to transmission peak degeneracies in accelerometers [47] and stabilizing noise at a nonlinear exceptional nexus [31]. Here, the NEP_5 with a complete basis offers a way out of the dilemma from its fundamental origins, i.e., noise is converged. Meanwhile, χ and the PF of NEP_5 can be further tuned by including nonreciprocal coupling (see Fig. S6 of the Supplemental Material [50]).

Another promising potential application of EPs is the chiral state transfer during the dynamical encirclement of EPs. Given the same initial state, the final state does not depend on the details of the trajectory but on the direction of the winding (clockwise or anticlockwise) [19–25,58]. Dynamical encirclement of a NEP_5 in the parameter space can also lead to chiral state transfer similar to conventional linear EPs. For demonstration purposes, the trajectory of encirclement (loop) is defined as $l_B + \delta x(t)$ and $\omega_B + \delta y(t)$. We set $\delta x(t) = r\cos(\tau 2\pi t/T)$ and $\delta y(t) = r\sin(\tau 2\pi t/T)$ with r representing the radius of the loop, T denoting the cycle period, and $\tau = \pm 1$ for the winding direction. Figures 3(a) and 3(b) show the steady-state frequencies versus δx and δy in the parameter space. The light red and light blue regions represent stable and unstable states, respectively. The system starts at a higher-frequency stable state, as marked by the bold green arrows. If $\tau = 1$ [see Fig. 3(a)], the state can adiabatically evolve to the lower frequency state, provided the circling process is slow

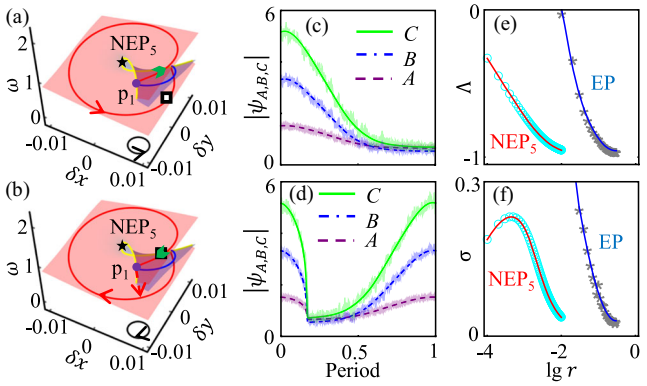

FIG. 3. Steady-state frequencies (a),(b) and the corresponding amplitudes (c),(d) around the NEP_5 (marked by the black star). In (c),(d), the solid green, dot-dashed blue, and dashed purple lines represent the cases without noise, and the corresponding light lines represent one typical simulation with noises. The chirality function Λ (e) and the corresponding standard deviations σ (f) are shown as a function of the encircling radius r. In (e),(f), the open cyan circles and gray aplstars are obtained from simulations of over 200 independent noises, and the red and blue lines are for eye guiding. The parameters are $\omega_B = 1.25$, $\omega_C = 1.59$, $l_B = 3.06$, $g_C = 1.40$, $\kappa_2 = 2.18$, $r = 0.01$, $T = 20000$, and $g_A = 5/(1 + |\psi_A|^2) - 3$. The amplitude of the noise is given by $D = 0.2$.

enough. In contrast, the state experiences a nonadiabatic transition at p_1 and evolves to the same state when winding in the clockwise direction [see Fig. 3(b)]. To quantify the chirality of a parametric path, we adopt [20] and extend the definition of chirality function as $\Lambda = \rho_{\mathrm{CW}}\rho_{\mathrm{CCW}}$, where the subscripts CW and CCW denote the clockwise and counterclockwise directions, respectively. Here the eigenstate population ρ describes the relative weight of the occupation coefficients and is defined as $\rho(t) = [|c_u(t)|^2 - |c_l(t)|^2]/[|c_u(t)|^2 + |c_l(t)|^2]$, where $c_{u,l}(t)$ represents the projection of the instantaneous state $|\boldsymbol{\psi}(t)\rangle$ on the upper or lower energy state. Figures 3(c) and 3(d) show the evolution of instantaneous amplitudes in the presence of noise (light lines), which are bounded around the case where there is no noise (bold lines). Different from circling other linear EPs, wherein the wave amplitude either exponentially increases or decreases (for passive systems) with time, here the wave amplitude maintains almost at the same order since the evolution is on the stable state surface. Figures 3(e) and 3(f) show the chirality function Λ and the corresponding standard deviations σ with a fixed noise as a function of the encircling radius r. Ideally, Λ should be -1 independent of r; in the presence of noise, Λ deviates from -1. Compared with circling an EP in a typical linear system [the blue line in Fig. 3(e)], the chirality function Λ [the red line in Fig. 3(e)] is much more robust against noise as it remains around -1 for a much smaller r. Moreover, the standard deviation σ converges [red line in Fig. 3(f)] as we approach the NEP_5. When r is large, the feedback mechanism is the dominant factor for the robustness of the chiral state transfer against noise; when r is small enough, both the feedback mechanism and the reviving of the complete basis contribute to the robustness. A more detailed analysis is provided in the Supplemental Material, Sec. 4 [50]. Here, the parametric steering process with an ultrasmall r enables the miniaturization of various key applications based on the chiral state transfer [21–25].

Conclusions.—In summary, we propose NEPs with the critical features of EPs. It is remarkable to find that the completeness of the eigenbasis at the NEP recovers in temporal dynamics, and this fact is also corroborated by a finite PF. The adverse consequences due to the loss of completeness are largely degraded from a fundamental aspect. Since nonlinearity fundamentally changes the dimension and dynamics of the system, we name it NEP to distinguish it from conventional EPs. Our model can be implemented within diverse classical and quantum systems, and we show their existence in the circuits in the Supplementary Material, Sec. 5. Besides the circuit system, other promising platforms include microwave cavities [6,16], exciton-polariton billiards [11], optical microcavities [8], coupled atom-cavity systems [9], cold atoms [59,60], nitrogen-vacancy centers [61], superconducting circuits [62], etc. [7,10,12,63]. The nonlinear EPs discussed in our work exhibit great potential in EP-related applications such as (quantum) sensing [13,16,31,47,63], chiral state transfer [19–22], etc. [64,65]. In addition, our findings will enrich the physics of the EPs of Bloch Hamiltonians under continuous deformations [66–68] and provide new insights into the nonlinear non-Hermitian systems [69].

The authors thank Chong Chen for helpful discussions. This work is supported by the National Key Research and Development Program of China (Grant No. 2022YFA1404900), the National Natural Science Foundation of China (Grants No. 12274330, No. 12274332), and the Knowledge Innovation Program of Wuhan-Shuguang (Grant No. 2022010801020125).

*ddwan@whu.edu.cn
†phmxiao@whu.edu.cn

[1] W. D. Heiss, J. Phys. A Math. Theor. **45**, 444016 (2012).
[2] I. Rotter, J. Phys. A Math. Theor. **42**, 153001 (2009).
[3] Y. Ashida, Z. Gong, and M. Ueda, Adv. Phys. **69**, 249 (2020).
[4] M. Berry, Czech. J. Phys. **54**, 1039 (2004).
[5] W. D. Heiss, J. Phys. A **37**, 2455 (2004).
[6] C. Dembowski, H.-D. Gräf, H. L. Harney, A. Heine, W. D. Heiss, H. Rehfeld, and A. Richter, Phys. Rev. Lett. **86**, 787 (2001).
[7] W. Tang, X. Jiang, K. Ding, Y.-X. Xiao, Z.-Q. Zhang, C. T. Chan, and G. Ma, Science **370**, 1077 (2020).
[8] S.-B. Lee, J. Yang, S. Moon, S.-Y. Lee, J.-B. Shim, S. W. Kim, J.-H. Lee, and K. An, Phys. Rev. Lett. **103**, 134101 (2009).
[9] Y. Choi, S. Kang, S. Lim, W. Kim, J.-R. Kim, J.-H. Lee, and K. An, Phys. Rev. Lett. **104**, 153601 (2010).
[10] B. Zhen, C. W. Hsu, Y. Igarashi, L. Lu, I. Kaminer, A. Pick, S.-L. Chua, J. D. Joannopoulos, and M. Soljačić, Nature (London) **525**, 354 (2015).
[11] T. Gao, E. Estrecho, K. Y. Bliokh, T. C. Liew, M. D. Fraser, S. Brodbeck, M. Kamp, C. Schneider, S. Höfling, Y. Yamamoto, F. Nori, Y. S. Kivshar, A. G. Truscott, R. G. Dall, and E. A. Ostrovskaya, Nature (London) **526**, 554 (2015).
[12] A. Regensburger, C. Bersch, M.-A. Miri, G. Onishchukov, D. N. Christodoulides, and U. Peschel, Nature (London) **488**, 167 (2012).
[13] H. Hodaei, A. U. Hassan, S. Wittek, H. Garcia-Gracia, R. El-Ganainy, D. N. Christodoulides, and M. Khajavikhan, Nature (London) **548**, 187 (2017).
[14] K. Ding, G. Ma, M. Xiao, Z. Q. Zhang, and C. T. Chan, Phys. Rev. X **6**, 021007 (2016).
[15] S. Wang, B. Hou, W. Lu, Y. Chen, Z. Q. Zhang, and C. T. Chan, Nat. Commun. **10**, 832 (2019).
[16] W. Chen, Kaya Özdemir, G. Zhao, J. Wiersig, and L. Yang, Nature (London) **548**, 192 (2017).
[17] L. Feng, Z. J. Wong, R.-M. Ma, Y. Wang, and X. Zhang, Science **346**, 972 (2014).
[18] H. Hodaei, M.-A. Miri, M. Heinrich, D. N. Christodoulides, and M. Khajavikhan, Science **346**, 975 (2014).

[19] J. Doppler, A. A. Mailybaev, J. Böhm, U. Kuhl, A. Girschik, F. Libisch, T. J. Milburn, P. Rabl, N. Moiseyev, and S. Rotter, Nature (London) **537**, 76 (2016).

[20] H. Nasari, G. Lopez-Galmiche, H. E. Lopez-Aviles, A. Schumer, A. U. Hassan, Q. Zhong, S. Rotter, P. LiKamWa, D. N. Christodoulides, and M. Khajavikhan, Nature (London) **605**, 256 (2022).

[21] H. Xu, D. Mason, L. Jiang, and J. G. E. Harris, Nature (London) **537**, 80 (2016).

[22] A. U. Hassan, B. Zhen, M. Soljačić, M. Khajavikhan, and D. N. Christodoulides, Phys. Rev. Lett. **118**, 093002 (2017).

[23] X. L. Zhang, T. Jiang, and C. T. Chan, Light Sci. Appl. **8**, 88 (2019).

[24] Y. Choi, C. Hahn, J. W. Yoon, S. H. Song, and P. Berini, Nat. Commun. **8**, 14154 (2017).

[25] B. Peng, Şahin Kaya Özdemir, M. Liertzer, W. Chen, J. Kramer, H. Yılmaz, J. Wiersig, S. Rotter, and L. Yang, Proc. Natl. Acad. Sci. U.S.A. **113**, 6845 (2016).

[26] H.-Z. Chen, T. Liu, H.-Y. Luan, R.-J. Liu, X.-Y. Wang, X.-F. Zhu, Y.-B. Li, Z.-M. Gu, S.-J. Liang, H. Gao, L. Lu, L. Ge, S. Zhang, J. Zhu, and R.-M. Ma, Nat. Phys. **16**, 571 (2020).

[27] D. Smirnova, D. Leykam, Y. Chong, and Y. Kivshar, Appl. Phys. Rev. **7**, 021306 (2020).

[28] V. V. Konotop, J. Yang, and D. A. Zezyulin, Rev. Mod. Phys. **88**, 035002 (2016).

[29] S. Assawaworrarit, X. Yu, and S. Fan, Nature (London) **546**, 387 (2017).

[30] H. Wang, S. Assawaworrarit, and S. Fan, Opt. Lett. **44**, 638 (2019).

[31] K. Bai, L. Fang, T.-R. Liu, J.-Z. Li, D. Wan, and M. Xiao, Natl. Sci. Rev. **10**, nwac259 (2022).

[32] S. Mandal, R. Banerjee, E. A. Ostrovskaya, and T. C. H. Liew, Phys. Rev. Lett. **125**, 123902 (2020).

[33] B. Zhu, Q. Wang, D. Leykam, H. Xue, Q. J. Wang, and Y. D. Chong, Phys. Rev. Lett. **129**, 013903 (2022).

[34] R. Banerjee, S. Mandal, and T. C. H. Liew, Phys. Rev. Lett. **124**, 063901 (2020).

[35] M. S. Kirsch, Y. Zhang, M. Kremer, L. J. Maczewsky, S. K. Ivanov, Y. V. Kartashov, L. Torner, D. Bauer, A. Szameit, and M. Heinrich, Nat. Phys. **17**, 995 (2021).

[36] D. Smirnova, D. Leykam, Y. Chong, and Y. Kivshar, Appl. Phys. Rev. **7**, 021306 (2020).

[37] S. Mittal, G. Moille, K. Srinivasan, Y. K. Chembo, and M. Hafezi, Nat. Phys. **17**, 1169 (2021).

[38] S. Mittal, E. A. Goldschmidt, and M. Hafezi, Nature (London) **561**, 502 (2018).

[39] S. Xia, D. Kaltsas, D. Song, I. Komis, J. Xu, A. Szameit, H. Buljan, K. G. Makris, and Z. Chen, Science **372**, 72 (2021).

[40] Z. Lin, A. Pick, M. Lončar, and A. W. Rodriguez, Phys. Rev. Lett. **117**, 107402 (2016).

[41] A. Pick, B. Zhen, O. D. Miller, C. W. Hsu, F. Hernandez, A. W. Rodriguez, M. Soljačić, and S. G. Johnson, Opt. Express **25**, 12325 (2017).

[42] H. Jing, K. Özdemir, H. Lü, and F. Nori, Sci. Rep. **7**, 3386 (2017).

[43] A. E. Siegman, Phys. Rev. A **39**, 1253 (1989).

[44] S.-Y. Lee, J.-W. Ryu, J.-B. Shim, S.-B. Lee, S. W. Kim, and K. An, Phys. Rev. A **78**, 015805 (2008).

[45] H. Wang, Y. H. Lai, Z. Yuan, M. G. Suh, and K. Vahala, Nat. Commun. **11**, 1610 (2020).

[46] C. Chen, L. Jin, and R.-B. Liu, New J. Phys. **21**, 083002 (2019).

[47] R. Kononchuk, J. Cai, F. Ellis, R. Thevamaran, and T. Kottos, Nature (London) **607**, 697 (2022).

[48] A. E. Siegman, *Lasers* (University Science Books, Sausalito, California, 1986).

[49] C. M. Bender and P. D. Mannheim, Phys. Lett. A **374**, 1616 (2010).

[50] See Supplemental Material at http://link.aps.org/supplemental/10.1103/PhysRevLett.130.266901, which includes Refs. [19–25,29–31,43–45,51–55], for further details.

[51] K. J. H. Peters and S. R. K. Rodriguez, Phys. Rev. Lett. **129**, 013901 (2022).

[52] M. Lyubarov, Y. Lumer, A. Dikopoltsev, E. Lustig, Y. Sharabi, and M. Segev, Science **377**, 425 (2022).

[53] T. J. Milburn, J. Doppler, C. A. Holmes, S. Portolan, S. Rotter, and P. Rabl, Phys. Rev. A **92**, 052124 (2015).

[54] J. Schindler, Z. Lin, J. M. Lee, H. Ramezani, F. M. Ellis, and T. Kottos, J. Phys. A Math. Theor. **45**, 444029 (2012).

[55] https://www.analog.com/en/design-center/design-tools-and-calculators/ltspice-simulator.html.

[56] H.-K. Lau and A. A. Clerk, Nat. Commun. **9**, 4320 (2018).

[57] A. Cerjan and A. D. Stone, Phys. Rev. A **90**, 013840 (2014).

[58] X.-L. Zhang, S. Wang, B. Hou, and C. T. Chan, Phys. Rev. X **8**, 021066 (2018).

[59] J. Li, A. K. Harter, J. Liu, L. de Melo, Y. N. Joglekar, and L. Luo, Nat. Commun. **10**, 855 (2019).

[60] Y. Jiang, Y. Mei, Y. Zuo, Y. Zhai, J. Li, J. Wen, and S. Du, Phys. Rev. Lett. **123**, 193604 (2019).

[61] W. Liu, Y. Wu, C.-K. Duan, X. Rong, and J. Du, Phys. Rev. Lett. **126**, 170506 (2021).

[62] M. Naghiloo, M. Abbasi, Y. N. Joglekar, and K. W. Murch, Nat. Phys. **15**, 1232 (2019).

[63] L. Ding, K. Shi, Q. Zhang, D. Shen, X. Zhang, and W. Zhang, Phys. Rev. Lett. **126**, 083604 (2021).

[64] M. Brandstetter, M. Liertzer, C. Deutsch, P. Klang, J. Schöberl, H. E. Türeci, G. Strasser, K. Unterrainer, and S. Rotter, Nat. Commun. **5**, 4034 (2014).

[65] B. Peng, K. Özdemir, S. Rotter, H. Yilmaz, M. Liertzer, F. Monifi, C. M. Bender, F. Nori, and L. Yang, Science **346**, 328 (2014).

[66] B. Zhen, C. W. Hsu, Y. Igarashi, L. Lu, I. Kaminer, A. Pick, S.-L. Chua, J. D. Joannopoulos, and M. Soljačić, Nature (London) **525**, 354 (2015).

[67] Y. Xu, S.-T. Wang, and L.-M. Duan, Phys. Rev. Lett. **118**, 045701 (2017).

[68] Z. Yang, C.-K. Chiu, C. Fang, and J. Hu, Phys. Rev. Lett. **124**, 186402 (2020).

[69] T. Karzig, C.-E. Bardyn, N. H. Lindner, and G. Refael, Phys. Rev. X **5**, 031001 (2015).